Journal of Materials Chemistry A

Accepted Manuscript

ROYAL SOCIETY OF CHEMISTRY

www.rsc.org/materialsA

Journal of Materials Chemistry A

RSCPublishing

ARTICLE

The effect of interstitial oxygen formation on the crystal lattice deformation in layered perovskite oxides for electrochemical devices

Cite this: DOI: 10.1039/x0xx00000x

Received 00th January 2012,
Accepted 00th January 2012

DOI: 10.1039/x0xx00000x

www.rsc.org/

Takashi Nakamura[a*], Yihan Ling[a], Koji Amezawa[a]

In order to understand the behaviour of the crystal lattice deformation induced by the interstitial oxygen formation in $La_2(Ni_{0.9}M_{0.1})O_{4+\delta}$ (M = Fe, Co, Cu), thermogravimetry, coulometric titration, and high temperature X-ray diffraction measurements were carried out in the temperature range between 873 to 1173 K and the $P(O_2)$ range between 10^{-24} to 1 bar. Compared with non-doped $La_2NiO_{4+\delta}$, $La_2(Ni_{0.9}Fe_{0.1})O_{4+\delta}$ and $La_2(Ni_{0.9}Co_{0.1})O_{4+\delta}$ have more interstitial oxygen while $La_2(Ni_{0.9}Cu_{0.1})O_{4+\delta}$ have less. Crystal structure at high temperatures was analyzed assuming the tetragonal symmetry, *I*4/*mmm*, for all compositions. With increasing interstitial oxygen concentration, the lattice parameter perpendicular to the perovskite layer increased and that parallel to the perovskite layer decreased. Consequently, the change of the cell volume by the interstitial oxygen formation was small, meaning macroscopic chemical expansion is small. Chemical and thermal deformation behaviour could be explained by assuming linear relation of the lattice constants to T and δ. Apparent and true thermal expansion coefficients and chemical expansion coefficient were calculated and compared with oxygen deficient perovskite- and fluorite-type oxides. It was found that the chemical expansion coefficient of La_2NiO_4-based oxides which is induced by the formation/annihilation of interstitial oxygen is smaller than that of perovskite- and fluorite-type oxides which is induced by the formation/annihilation of oxygen vacancy.

Introduction

K_2NiF_4-type oxides have gained great attention as a promising component for the electrochemical devices because they show excellent properties such as mixed oxide ion and electron conductivity, catalytic activity, oxygen storage capacity and oxygen diffusivity.[1-5] The origin of these electrochemical properties is the interstitial oxygen in K_2NiF_4 structure.[6-9] Interstitial oxygen formation is expressed by

$$\frac{1}{2}O_2(g) + V_i^{\times} \rightarrow O_i'' + 2h^{\cdot} \quad (1)$$

where defect species are shown by the Kröger-Vink notation.[10] Interstitial oxygen and holes plays an important role for above-mentioned electrochemical properties of the K_2NiF_4-type oxides. Figure 1 shows the crystal structure of La_2NiO_4 with tetragonal symmetry. Perovskite and rock salt structures are alternately stacked. Neutron diffraction measurement revealed that the interstitial oxygen in $La_2NiO_{4+\delta}$ is preferentially located at the centre of the pseudo-tetrahedron of lanthanum in the rock salt structure.[11] Fast ionic conduction path extends through the rock salt layers. The anisotropic oxygen diffusion was confirmed by theoretical calculations and experiments using single crystal or epitaxial film specimens.[12-14] Since interstitial oxygen easily migrate through rock salt structure, the activation energy of oxygen diffusivity of K_2NiF_4-type oxides is smaller than that of perovskite- and fluorite-type mixed conductor which has oxygen vacancy as a ionic carrier.[2] Because of excellent electrochemical properties, K_2NiF_4-type oxides are applied to cathode of solid oxide fuel cells, membrane reactors, oxygen permeation membranes, and catalyst for the oxygen reduction and oxygen evolution reactions.[15-18]

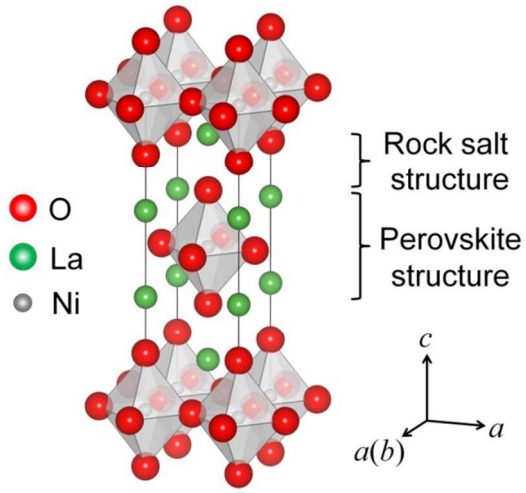

Figure 1. Crystal structure of tetragonal La_2NiO_4

During the operation of the electrochemical devices, the components can be exposed to severe conditions such as high temperatures, strongly reducing or oxidizing atmospheres, and large chemical potential or temperature gradient. Under such conditions, the components may be deformed by the formation and/or annihilation of defect species. Since the unexpected deformation can cause serious damage during operation, fundamental knowledge about the chemical deformation behaviour is important to design the reliable electrochemical devices and to determine suitable operating conditions. Because of these reason, chemical and thermal expansion behaviour of perovskite- and fluorite-type oxides has been widely studied. The lattice parameters of doped ceria increase with increasing oxygen vacancy concentration.[19-21] The causes of chemical expansion in ceria-based oxides are considered to be the balance of the electrostatic effect and the change of ionic radius.[22] Chemical expansion under reducing atmosphere was also observed in perovskite-type oxides.[23-26] $LaMnO_3$ shows not only the reduction expansion but also unique chemical deformation behaviour under high $P(O_2)$ condition which is caused by the creation and annihilation of new crystal lattice.[27, 28]

Contrary to the lattice deformation of perovskite- and fluorite-type oxides which is induced by the oxygen vacancy formation, the effect of the interstitial oxygen formation on the lattice deformation of layered perovskite oxides is not clear yet except some earlier works[3, 29, 30] For the development of high-performance and reliable devices, it is necessary to understand chemical and thermal deformation behaviour of the component. In the present work, the authors try to evaluate the crystal lattice deformation behaviour of $La_2(Ni_{0.9}M_{0.1})O_{4+\delta}$ (M = Fe, Co and Cu) and establish the thermal and chemical deformation model. For that purpose, thermogravimetry (TG), coulometric titration (CT) and high temperature X-ray diffraction measurements were carried out at 873-1173 K in N_2-O_2 atmosphere. Interstitial oxygen concentration was determined by TG and CT measurements and lattice parameters were calculated from the XRD patterns. The crystal lattice deformation by the variation of temperature and the interstitial oxygen concentration is evaluated. True and apparent thermal expansion coefficients and chemical expansion coefficient of La_2NiO_4-based oxides were calculated and compared with those of oxygen deficient perovskite- and fluorite-type oxides.

Experimental

Sample preparation

$La_2(Ni_{0.9}Fe_{0.1})O_{4+\delta}$ (LNO-Fe10), $La_2(Ni_{0.9}Co_{0.1})O_{4+\delta}$ (LNO-Co10) and $La_2(Ni_{0.9}Cu_{0.1})O_{4+\delta}$ (LNO-Cu10) were synthesized by a solid state reaction method. La_2O_3 (99.99%, KANTO CHEMICAL CO., INC), NiO (99.95%, KANTO CHEMICAL CO., INC), Fe_2O_3 (99.9%, Koujundo Chemical Laboratory Co., Ltd.), CoO (99.9%, Koujundo Chemical Laboratory Co., Ltd.), CuO (99.9%, RARE METALLIC Co., Ltd.) were mixed in a proper cation ratio. They were mixed by a planetary ball mill at 300 rpm for 3 h with ethanol. After drying, mixed powers were sintered at 1523 K for 10 h 2 times with intermediate grindings. No peak of secondary phase was observed by XRD

Evaluation of the interstitial oxygen concentration

Detail procedure of the TG and the CT was shown in our previous study.[6] Oxygen content variation under $P(O_2)$ range from 10^{-4} to 1 bar was measured by TG measurement using electronic microbalances (Cahn D200 and Sartorius M25DP), and that in $P(O_2)$ < 10^{-3} bar condition was evaluated by the CT using YSZ electrochemical cell. For TG measurement, the change in the oxygen content was determined from the variation of the weight of the specimen, Δw_s,

$$\Delta\delta = \frac{M_s}{M_O}\frac{\Delta w_s}{w_s} \quad (2)$$

where $\Delta\delta$, M_s, M_O, and w_s are the variation of oxygen nonstoichiometry, the formula weight of the sample and oxygen atom, and the weight of the specimen, respectively. For the CT measurement, the amount of oxygen in the specimen was controlled by the electric charge passed through the cell. After a specified amount of electric charge was passed, $\Delta\delta$ was calculated by the equation

$$\Delta\delta = \frac{C}{2FM_s} \quad (3)$$

where C and F is the total amount of electric charge and the Faraday constant, respectively. Corresponding equilibrium oxygen partial pressure was determined from the electromotive force between inside and outside of the cell.

The absolute value of the oxygen content was determined from the weight change of the specimen by the decomposition in H_2 atmosphere. It is confirmed by XRD measurement that the sample was decomposed to lanthanum oxide and metallic state of Ni and dopant after the H_2 treatment which is expressed by

$$La_2(Ni_{0.9}M_{0.1})O_{4+\delta} \rightarrow La_2O_3 + 0.9Ni + 0.1M + \frac{2+2\delta}{2}O_2(g) \quad (4)$$

One mole of the sample will release $(2+2\delta)/2$ mole of oxygen gas by the reduction. Weight loss measurements by the reduction of the sample were applied to determine the oxygen content of the specimen by the preceding works too.[6, 7]

High temperature XRD measurement

High temperature XRD measurements were carried out with D8 Advance X-ray diffractometer (Bruker AXS) using Cu-K_α radiation. The diffraction patterns between 10-60° in 2 theta were obtained with the angular step width of 0.02°. The X-ray diffraction measurements were carried out in the temperature range between 873-1173 K, and the $P(O_2)$ range between 10^{-4} to 1 bar. Temperature and $P(O_2)$ around the specimen were controlled by a Pt heater and N_2-O_2 gas-mixtures, respectively. $P(O_2)$ of inlet and outlet gases was monitored by the YSZ oxygen sensor. The lattice parameters were obtained from the diffraction patterns by Whole Powder Pattern Decomposition (WPPD) with analytical software TOPAS.[31]

Results and Discussion

Interstitial oxygen formation in $La_2(Ni_{0.9}M_{0.1})O_{4+\delta}$ (M = Fe, Co, Cu)

Figures 2, 3 and 4 show nonstoichiometric oxygen content variation of LNO-Fe10, LNO-Co10 and LNO-Cu10, respectively. In the figures, closed and open symbols show the results from TG and CT, respectively. It is confirmed that the results from TG and CT show good agreement. This supports the validity of our TG and CT measurements. The amount of excess oxygen in La_2NiO_4-based oxides increases with increasing $P(O_2)$ and decreasing T. While LNO-Fe10 and LNO-Co10 shows only oxygen excess composition,

LNO-Cu10 shows small oxygen deficiency under low $P(O_2)$ condition. The oxygen deficiency under low $P(O_2)$ condition was also confirmed in $(La,Sr)_2NiO_{4+\delta}$ and $La_2CuO_{4+\delta}$.[6, 32] The effect of dopant species on oxygen nonstoichiometric behaviour will be discussed in the next paragraph based on defect chemistry. In Figs 3 and 4, the slope of $4+\delta$ vs. $\log P(O_2)$ curve becomes small near the stoichiometric oxygen content ($4+\delta \approx 4$), indicating the plateau like behaviour of $4+\delta$ vs. $\log P(O_2)$ near the stoichiometric oxygen content. This is consistent with the thermodynamic consideration of nonstoichiometric compounds.[33] According to our defect chemical analysis on $La_{2-x}Sr_xNiO_{4+\delta}$ and $Nd_{2-x}Sr_xNiO_{4+\delta}$, interstitial oxygen and oxygen vacancy hardly coexist in the K_2NiF_4-type oxide.[6, 34] Therefore, the amount of oxygen hypo-stoichiometry, δ, can be considered as the concentration of interstitial oxygen in this system.

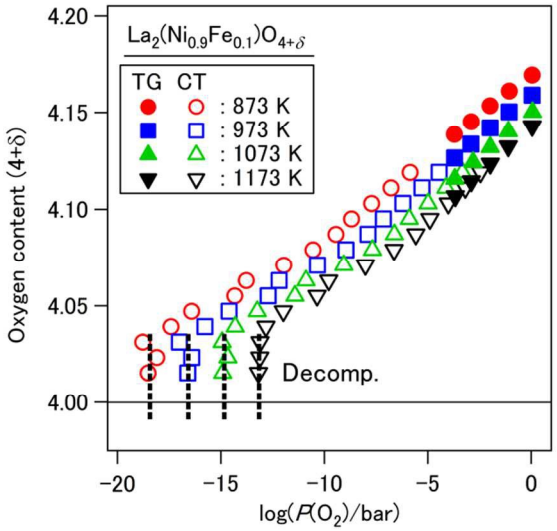

Figure 2. Oxygen content variation of $La_2(Ni_{0.9}Fe_{0.1})O_{4+\delta}$. Closed and open symbols were measured by TG and CT, respectively.

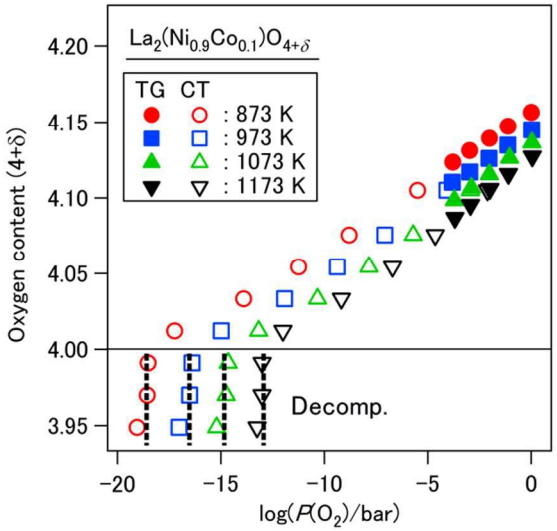

Figure 3. Oxygen content variation of $La_2(Ni_{0.9}Co_{0.1})O_{4+\delta}$. Closed and open symbols were measured by TG and CT, respectively.

The oxygen content of $La_2NiO_{4+\delta}$, LNO-Fe10, LNO-Co10 and LNO-Cu10 at 1073 K are summarized in Figure 5 to evaluate the effect of B-site doping. The concentration of interstitial oxygen strongly depends on the dopant species. Compared with non-doped $La_2NiO_{4+\delta}$, LNO-Fe10 and LNO-Co10 showed larger oxygen hypo-stoichiometry, while LNO-Cu10 showed smaller. This can be semi-quantitatively explained by the defect chemical consideration. The difference of oxygen content between LNO-Fe10 and $La_2NiO_{4+\delta}$ is about 0.05 under the same temperature and $P(O_2)$ condition. Plausible defect structure of LNO-Fe10 is that the Fe in LNO-Fe10 is trivalent and the charge neutrality was maintained by the interstitial oxygen formation

$$Fe_2O_3 + V_i^{\times} \rightarrow 2Fe_{Ni}^{\cdot} + O_i'' + 2O_O^{\times} \qquad (5)$$

Here, the balance of La-site is omitted. The presence of trivalent Fe in $La_2NiO_{4+\delta}$ was confirmed by Mössbauer spectroscopy[7].

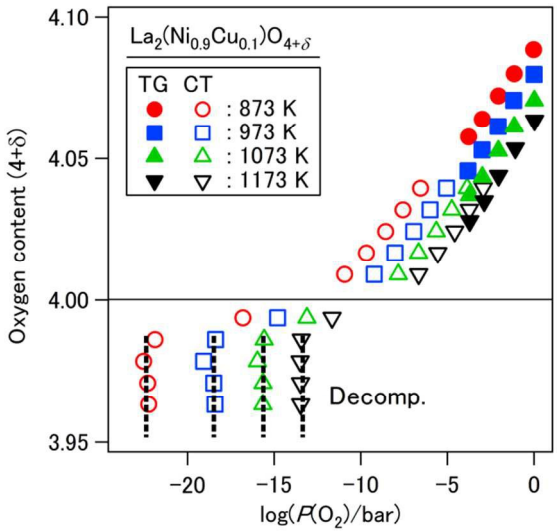

Figure 4. Oxygen content variation of $La_2(Ni_{0.9}Cu_{0.1})O_{4+\delta}$. Closed and open symbols were measured by TG and CT, respectively.

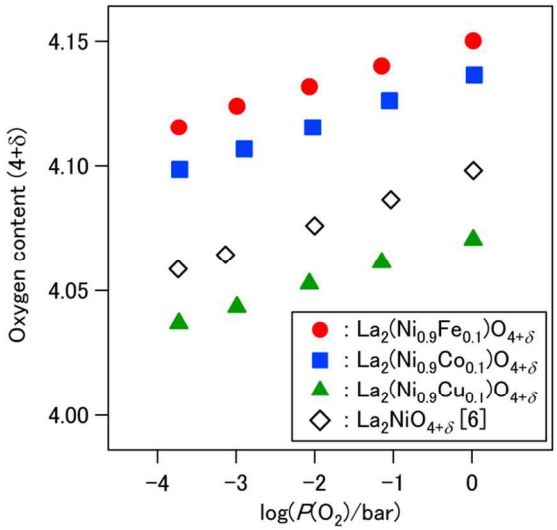

Figure 5. Comparison of oxygen content of $La_2NiO_{4+\delta}$[6] and $La_2(Ni_{0.9}M_{0.1})O_{4+\delta}$ (M = Fe, Co, Cu) at 1073 K.

The difference of oxygen content between LNO-Co10 and $La_2NiO_{4+\delta}$ is about 0.03 under the same temperature and $P(O_2)$ condition. Two possibilities are considered in this case, one is Co is not fully trivalent but the mixed state of bivalent and trivalent, the other is Co is trivalent and charge neutrality was maintained by the formation of interstitial oxygen and electron

$$Co_2O_3 + nV_i^{\times} \rightarrow 2Co_{Ni}^{\cdot} + nO_i'' + 2(1-n)e' + (3-n)O_O^{\times} \quad (6)$$

Although the plateau of the 4+δ vs. log$P(O_2)$ curve may be expected at Ni mean valence of 2 for LNO-Fe10 and LNO-Co10, such a plateau behaviour was not observed around 4+$\delta \approx 4.05$. This may suggest unfilled band state at Ni mean valence of 2 in LNO-Fe10 and LNO-Co10. Contrary to LNO-Fe10 and LNO-Co10, LNO-Cu10 showed smaller oxygen content compared with $La_2NiO_{4+\delta}$. One possibility of this behaviour is the presence of monovalent Cu and corresponding disappearance of the interstitial oxygen. However, monovalent Cu in K_2NiF_4-type oxides is questionable since almost stoichiometric La_2CuO_4 is a stable phase. The other possibility is the structural restriction for the insertion of oxygen into the rock salt structure. Strongly distorted CuO_6 was reported (Cu-O along *c*: 2.43 Å, Cu-O along *ab*: 1.9 Å), while the distortion of NiO_6 was not so big (Ni-O along *c*: 2.28 Å, Ni-O along *ab*: 2.0 Å).[35, 36] This is caused by the difference of the electronic structure, *i.e.*, much stronger Jahn-Teller distortion arises in $Cu^{2+}O_6$ (*d*9 state) than in $Ni^{2+}O_6$ (*d*8 state). The difference of the MO_6 structure can strongly affect to the capacity of interstitial oxygen into the rock salt layer.

In Figures 2-4, decomposition of the specimens due to the reduction was shown as dashed lines at each temperature. The decomposition $P(O_2)$ due to the reduction are summarized in Figure 6 and compared with that of $La_2NiO_{4+\delta}$. As shown in the figure, decomposition $P(O_2)$ of $La_2NiO_{4+\delta}$ has some range. While LNO-Cu10 shows slightly better reduction tolerance than LNO-Fe10 and LNO-Co10, observed decomposition $P(O_2)$ of all specimen studied here is within the range of reported data.[6, 37, 38] This indicates that 10 mol% doping of Fe, Co and Cu on Ni-site does not affect the tolerance to the reduction decomposition.

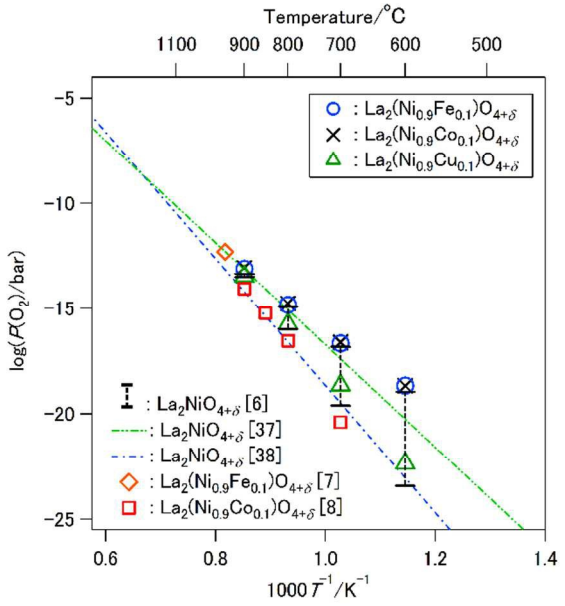

Figure 6. van't Hoff plot of the decomposition $P(O_2)$ of $La_2(Ni_{0.9}M_{0.1})O_{4+\delta}$ (M = Fe, Co, Cu). Reported decomposition $P(O_2)$ of La_2NiO_4-based oxides are also shown in the figure.[6-8, 37, 38]

Crystal lattice deformation due to the interstitial oxygen formation in $La_2(Ni_{0.9}M_{0.1})O_{4+\delta}$ (M = Fe, Co, Cu)

Figure 7 shows the obtained XRD patterns of LNO-Fe10 in 1 bar O_2 at room temperature to 1173 K. It is clearly confirmed that the XRD peaks shift to the lower angle with increasing temperature, which is caused by the thermal expansion. Due to the analogy of the high T_c superconductor, La_2CuO_4, crystal structure of $La_2NiO_{4+\delta}$ have been widely studied. Various structure models are proposed for $La_2NiO_{4+\delta}$ near or below the ambient temperature, *e.g.*, orthorhombic symmetries (*Fmmm*, *Bmab*), tetragonal symmetries (*I*4/*mmm*, *F*4/*mmm*, $P4_2/ncm$), and Phase separation.[11, 36, 38-42] On the other hand, the tetragonal symmetry, *I*4/*mmm*, is suggested at higher temperatures.[39, 41, 42]

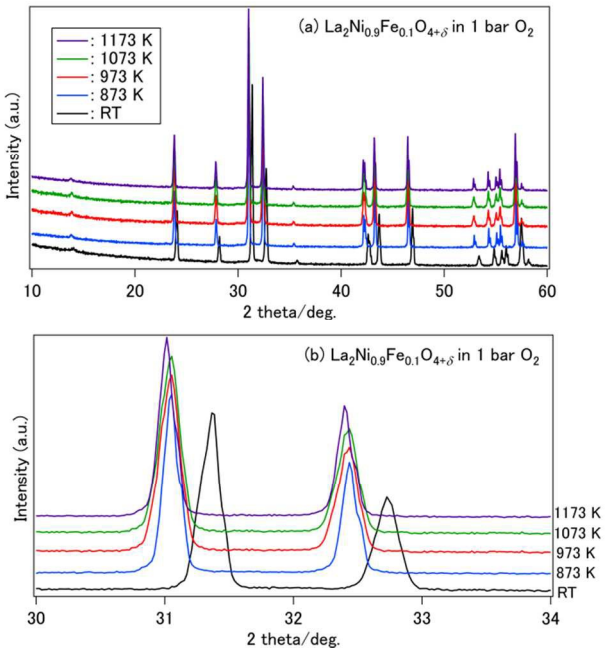

Figure 7. XRD patterns of $La_2(Ni_{0.9}Fe_{0.1})O_{4+\delta}$ measured in 1 bar O_2 at room temperature to 1173 K. (a) whole XRD spectra and (b) around the highest peak.

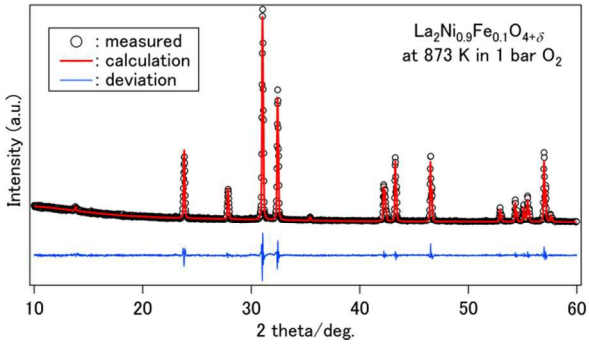

Figure 8. XRD pattern of $La_2(Ni_{0.9}Fe_{0.1})O_{4+\delta}$ measured at 873 K in 1 bar O_2 and the results of WPPD fitting. R_{wp} and GOF were 5.78 and 1.58, respectively.

In this study, the authors found that the diffraction patterns for all composition can be indexed by the tetragonal symmetry, *I*4/*mmm*, and no obvious advantages of orthorhombic symmetry model. Therefore, the authors calculate the lattice parameters assuming tetragonal symmetry. *a* and *c* represent the lattice parameter along AO and ABO_3 layers and that perpendicular to these layers, respectively. To obtain the lattice parameters, WPPD fitting was carried out on XRD patterns measured at 873-1173 K in 10^{-4} to 1 bar O_2 using TOPAS[31]. Figure 8 shows XRD pattern of LNO-Fe10 measured at 873 K in 1 bar O_2 and the result of WPPD fitting. R_{wp} and GOF were 5.78 and 1.58, respectively. Figures 9-11 show *a*, *c*, and the cell volume of LNO-Fe10, LNO-Co10 and LNO-Cu10 as functions of δ and *T*. As shown in the figures, anisotropic chemically-induced deformation was observed. As δ increased, *a*

decreased and c increased, as a consequence, the cell volume slightly increased with δ. This anisotropic chemical deformation is the unique phenomena of oxygen hypo-stoichiometric layered perovskite-type oxides, which is completely different from the chemical deformation of oxygen deficient perovskite- and fluorite-type oxides. The small chemical expansion behaviour was also reported by the dilatometric measurements.[3] The same tendency of the chemical deformation was confirmed in all compositions studied here.

As shown in Figs 9-11, local lattice deformation due to T and δ variation is significant in La_2NiO_4-based oxides. The formulation of the crystal lattice deformation behaviour is shown as follows. Because the lattice parameters are essentially determined by the oxygen content and temperature, a and c can be expressed by the total differential form by

$$a(T,\delta) = a_{\mathrm{ref}} + \left(\frac{\partial a}{\partial T}\right)_{\delta} \Delta T + \left(\frac{\partial a}{\partial \delta}\right)_{T} \Delta\delta \quad (7)$$

$$c(T,\delta) = c_{\mathrm{ref}} + \left(\frac{\partial c}{\partial T}\right)_{\delta} \Delta T + \left(\frac{\partial c}{\partial \delta}\right)_{T} \Delta\delta \quad (8)$$

where a_{ref} and c_{ref} are the lattice parameters at an arbitrary reference state. Partial differentiation terms, chemical and thermal expansion coefficients, of a are obtained from the a vs. T plots at the same δ and the a vs. δ plots at constant T. In this study, it is assumed that the partial differentiation terms are independent of T and δ, meaning the lattice parameters linearly depend on δ and T. Partial differentiation terms in Eqs. 7 and 8 are calculated, and the average values in the temperature range of 873-1173 K are summarized in Table 1. The calculated results of Eqs. 7 and 8 using the parameters in Table 1 are shown in Figs. 9-11. The deformation model with a linear approximation can explain the chemically and thermally induced crystal lattice deformation of $La_2NiO_{4+\delta}$ based oxides. By the deformation model proposed in this study, one can estimate the structural changes of K_2NiF_4-type oxides under given atmosphere and temperature.

The origin of the strongly anisotropic chemical and thermal deformation is estimated as follows. As shown in Fig. 1, it is considered that a is mainly determined by Ni-O bonding in NiO_6 octahedron and c is determined by both rock salt and perovskite structures. From the difference of the thermal expansion along a and c axes, *i.e.* $(\partial c/\partial T)_{\delta}$ is almost 10 times larger than $(\partial a/\partial T)_{\delta}$, it can be expected that the rock salt structure is easily deformed compared with Ni-O bonding in NiO_6. Then, the structure of La_2NiO_4-baed oxides is interpreted as the alternate stacking of the strong NiO_6 layer and relatively soft rock salt layer. In La_2NiO_4-based oxides, Ni $3d$ and O$2p$ orbital are strongly hybridized and form 2-dimensional electronic conduction path. When interstitial oxygen is formed, hole is concurrently created in Ni-O band as shown in Eq. 1 and the Fermi level shift to the middle of the Ni-O band. Consequently, the covalency and bonding of Ni-O hybridized orbital becomes stronger and result in the slight decrease of a with δ. On the other hand, rock salt layer accepts interstitial oxygen and their structure will be relaxed by the electrostatic effect and loss of the free volume. The relaxation of the rock salt structure is allowed along c axis because ab plane is confined by the continuous NiO_6 connections. This can be quantitative explanation of c increase with δ.

Table 1. Partial differentiation terms for Eqs. 7 and 8

Sample	$\left(\frac{\partial a}{\partial T}\right)_{\delta}$	$\left(\frac{\partial a}{\partial \delta}\right)_{T}$	$\left(\frac{\partial c}{\partial T}\right)_{\delta}$	$\left(\frac{\partial c}{\partial \delta}\right)_{T}$
$La_2(Ni_{0.9}Fe_{0.1})O_{4+\delta}$	3.0×10^{-5}	-0.081	2.1×10^{-4}	0.84
$La_2(Ni_{0.9}Co_{0.1})O_{4+\delta}$	3.1×10^{-5}	-0.051	2.2×10^{-4}	0.62
$La_2(Ni_{0.9}Cu_{0.1})O_{4+\delta}$	3.2×10^{-5}	-0.051	1.8×10^{-4}	0.70

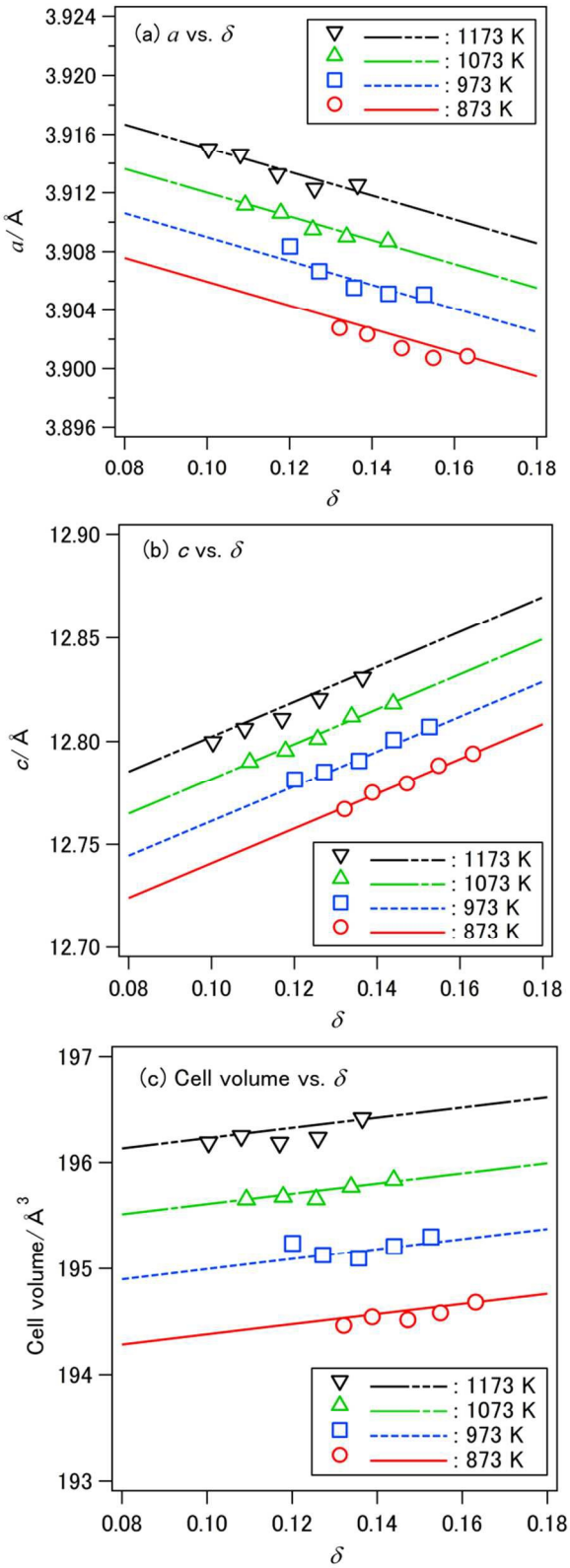

Figure 9. Lattice parameters and the cell volume of $La_2(Ni_{0.9}Fe_{0.1})O_{4+\delta}$ as functions of T and δ. Calculated results of Eqs. 7 and 8 using the parameters shown in Table 1 are shown as lines

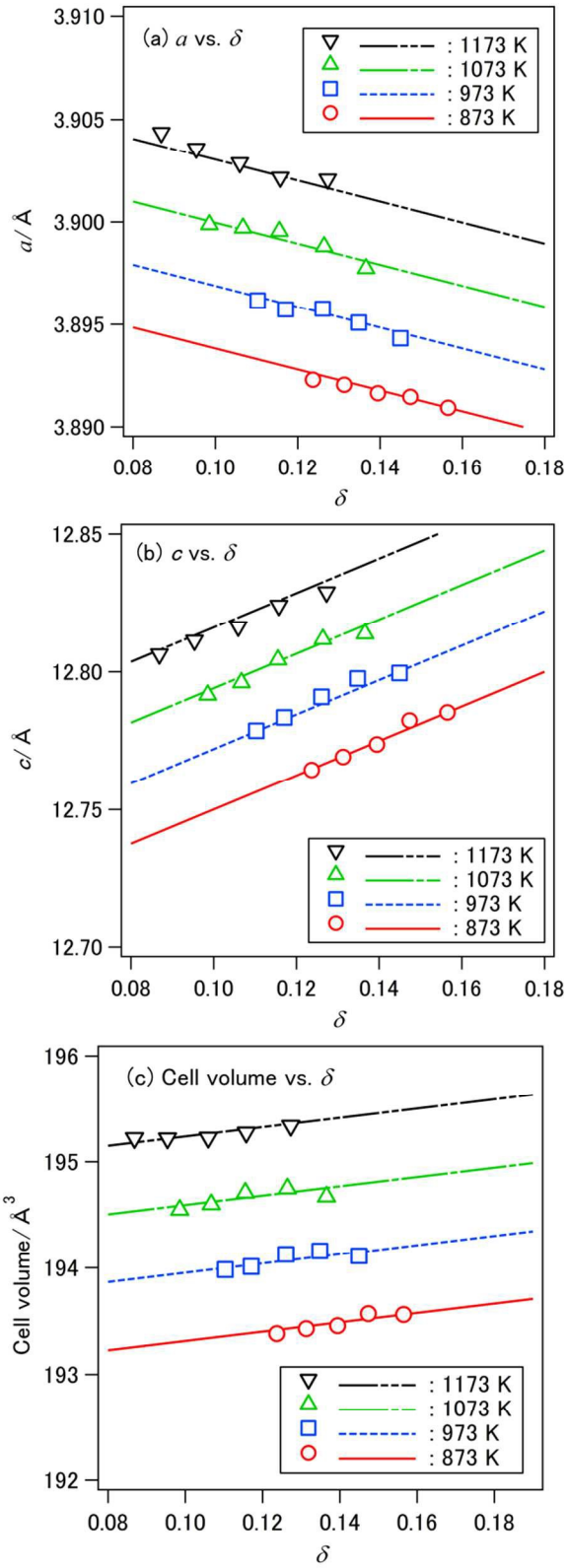

Figure 10. Lattice parameters and the cell volume of $La_2(Ni_{0.9}Co_{0.1})O_{4+\delta}$ as functions of T and δ. Calculated results of Eqs. 7 and 8 using the parameters shown in Table 1 are shown as lines

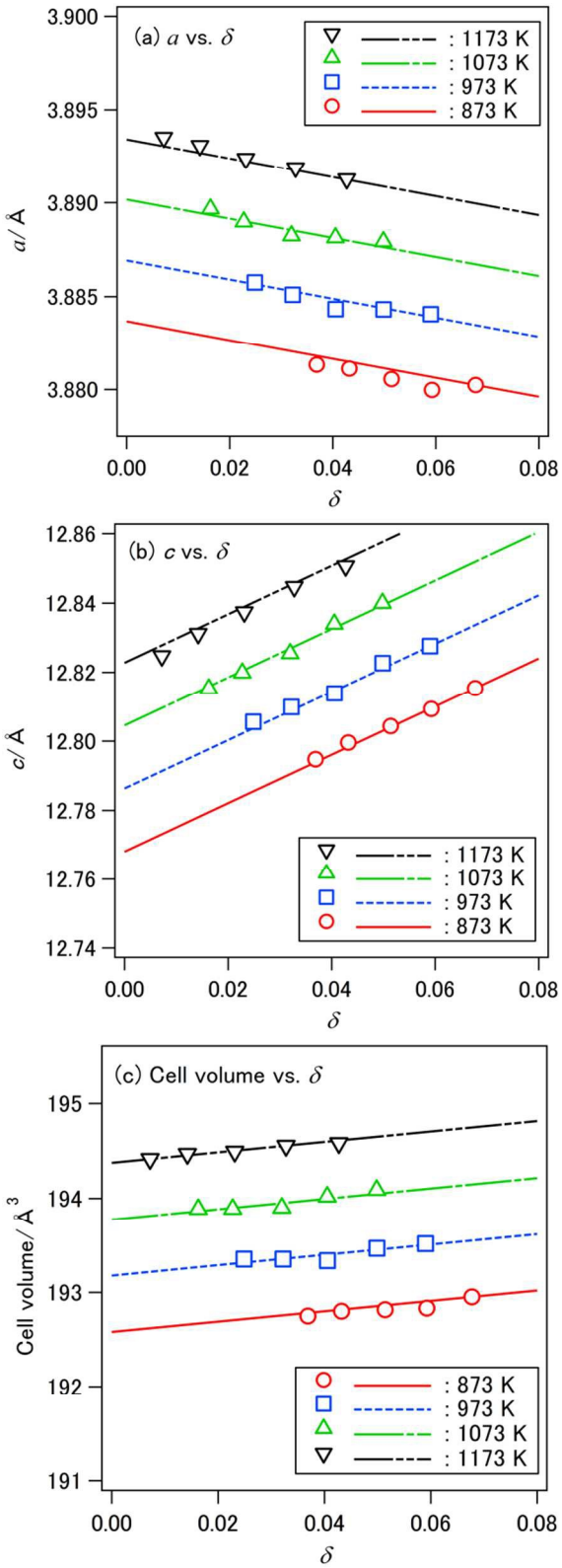

Figure 11. Lattice parameters and the cell volume of $La_2(Ni_{0.9}Cu_{0.1})O_{4+\delta}$ as functions of T and δ. Calculated results of Eqs. 7 and 8 using the parameters shown in Table 1 are shown as lines

Thermal and chemical expansion coefficients of $La_2(Ni_{0.9}M_{0.1})O_{4+\delta}$ (M = Fe, Co, Cu)

As shown in Figs 2-4, the oxygen content of $La_2NiO_{4+\delta}$ based oxides varies with temperature even in a fixed atmospheric condition. Therefore, thermal expansion in a given atmosphere is the apparent thermal expansion which contains both thermally-induced and chemically-induced deformations. Apparent linear thermal expansion coefficient, α_{app}, can be calculated from the slope of the (cell volume)$^{1/3}$ vs. T in a given atmospheric condition, while true linear thermal expansion coefficient, $\alpha_{true,}$ can be calculated from the slope of the (cell volume)$^{1/3}$ vs. T under given oxygen content. α_{app}, α_{true} and chemical expansion coefficients, α_{chem} (=ε/δ), of La_2NiO_4-based oxides are summarized in Table.2. For the comparison, expansion coefficients of perovskite- and fluorite-type oxides are also summarized in Table 2.[19-21, 24-26, 29, 30, 43-48] Compared with perovskites and fluorites whose oxygen defect is oxygen vacancies, La_2NiO_4-based oxides show much smaller α_{chem}. That result in the small difference between α_{app} and α_{true}. Layered perovskite oxides show much smaller chemical deformation compared with well known SOFC components and oxygen permeation membrane substrates such as $(La,Sr)CoO_{3-\delta}$, $(La,Sr)(Co,Fe)O_{3-\delta}$, $(Ba,Sr)(Co,Fe)O_{3-\delta}$ and CeO_2-based oxides. Small chemical deformation of layered perovskites is a preferable feature to fabricate reliable electrochemical devices. For instance, strong stress is expected in oxygen permeation membranes because the membranes are exposed to the large μ_O gradient under the operating conditions. Local oxygen content and corresponding crystal structure changes depending on the μ_O distribution in the membrane. Therefore, significant chemically-induced stress (strain) arises in high α_{chem} membrane substrates. On the other hand, layered perovskite membrane is almost free from the chemically-induced stress even under large oxygen chemical potential gradient. In addition to excellent electrochemical properties, small α_{chem} is a strong advantage of the layered perovskite oxides.

Table 2. Apparent and true linear thermal expansion coefficients and chemical expansion coefficients of $La_2(Ni_{0.9}M_{0.1})O_{4+\delta}$ (M = Fe, Co, Cu) and perovskite- and fluorite-type oxides.

Sample	α_{app} / K^{-1} (T range, atm.)	α_{true} / K^{-1} (T range, δ)	α_{chem} (δ range, T range)	References
$La_2(Ni_{0.9}Fe_{0.1})O_{4+\delta}$	9.77×10^{-6} (873-1173 K, 1 bar O_2)	9.93×10^{-6} (873-1173 K, 0.12)	9.2×10^{-3} (0.10-0.16, 873-1173 K)	This work
$La_2(Ni_{0.9}Co_{0.1})O_{4+\delta}$	10.1×10^{-6} (873-1173 K, 1 bar O_2)	11.1×10^{-6} (873-1173 K, 0.12)	6.9×10^{-3} (0.087-0.16, 873-1173 K)	This work
$La_2(Ni_{0.9}Cu_{0.1})O_{4+\delta}$	9.42×10^{-6} (873-1173 K, 1 bar O_2)	10.4×10^{-6} (873-1173 K, 0.04)	9.4×10^{-3} (0.0072-0.068, 873-1173 K)	This work
$La_2NiO_{4+\delta}$	11.0×10^{-6} (873-1173 K, 1 bar O_2)	11.6×10^{-6} (873-1173 K, 0.08)	4.4×10^{-3} (0.049-0.12, 873-1173 K)	29
$Nd_2NiO_{4+\delta}$	11.6×10^{-6} (873-1173 K, 1 bar O_2)	11.2×10^{-6} (873-1173 K, 0.11)	-1.8×10^{-3} (0.063-0.15, 873-1173 K)	30
$La_{0.6}Sr_{0.4}FeO_{3-\delta}$	17.1×10^{-6} (873-1173 K, air)	11.1×10^{-6} (773-1173 K, 0)	0.027 (0.017-0.12, 1073 K)	24, 43
$La_{0.6}Sr_{0.4}CoO_{3-\delta}$	20.5×10^{-6} (303-1273 K, air)	-	0.018 (0.012-0.075, 869-1165 K)	25, 44
$La_{0.6}Sr_{0.4}Co_{0.2}Fe_{0.8}O_{3-\delta}$	15.3×10^{-6} (373-873 K, air)	16.0×10^{-6} (300-1100 K, 0)	0.023 (0.055-0.15, 1073 K)	26, 45
$Ba_{0.5}Sr_{0.5}Co_{0.2}Fe_{0.8}O_{3-\delta}$	24.0×10^{-6} (873-1123 K, 1 bar O_2)	20.8×10^{-6} (873-1173 K, 0.72)	0.019 (0.70-0.82, 1073 K)	46, 47
$Ce_{0.8}Gd_{0.2}O_{2-\delta}$	12.4×10^{-6} (298-1273 K, air)	-	0.084 (0-0.07, 1073 K)	20, 21
$Ce_{0.8}Sm_{0.2}O_{2-\delta}$	11.1×10^{-6} (298-1273 K, air)	-	0.064 (0-0.04, 1073 K)	19, 48

Conclusions

The oxygen content variation and crystal structure of $La_2(Ni_{0.9}M_{0.1})O_{4+\delta}$ (M = Fe, Co, Cu) was measured by thermogravimetry, coulometric titration and high temperature X-ray diffraction measurements in N_2-O_2 atmosphere at 873-1173 K. Compared with non-doped $La_2NiO_{4+\delta}$, $La_2(Ni_{0.9}Fe_{0.1})O_{4+\delta}$ and $La_2(Ni_{0.9}Co_{0.1})O_{4+\delta}$ shows higher interstitial oxygen concentration and $La_2(Ni_{0.9}Cu_{0.1})O_{4+\delta}$ shows lower concentration, indicating better electrochemical performance of Fe and Co doped $La_2NiO_{4+\delta}$. As the amount of excess oxygen increases, the lattice parameter perpendicular to the perovskite layer increases and that parallel to the layer decreases. Consequently, cell volume is slightly increases with interstitial oxygen concentration. The thermally-induced and chemically-induced crystal lattice deformation can be expressed by the model with a linear approximation. From the dependence of the lattice parameters on T and δ, apparent and true thermal expansion coefficients and chemical expansion coefficient were calculated. The chemical expansion coefficient of layered perovskites is much smaller than that of perovskite or fluorite type oxides. Better tolerance and mechanical compatibility are expected for La_2NiO_4-based oxides.

Acknowledgements

This research was partly supported by the Institute of Multidisciplinary Research of Advanced Materials, Tohoku University.

Notes and references

[a] Institute of Multidisciplinary Research for Advanced Materials, Tohoku University.

1 S. J. Skinner, J. A. Kilner, *Solid State Ionics*, 2000, **135**, 709.
2 E. Boehm, J. M. Bassat, P. Dordor, F. Mauvy, J. C. Grenier, Ph. Stevens, *Solid State Ionics,* 2005, **176**, 2717.
3 V. V. Kharton, A. V. Kovalevsky, M. Avdeev, E. V. Tsipis, M. V. Patrakeev, A. A. Yaremchenko, E. N. Naumovich, J. R. Frade, *Chem. Mater*., 2007, **19**, 2027.
4 S. -Y. Jeon, M. -B. Choi, H. -N. Im, J. -H. Hwang, S. -J. Song, *J. Phys. Chem. Solids*. 2012, **73**, 656.
5 C. Tealdi, C. Ferrara, P. Mustarelli, M. S. Islam, *J. Mater. Chem*., 2012, **22**, 8969.
6 T. Nakamura, K. Yashiro, K. Sato, J. Mizusaki, *Solid State Ionics*, 2009, **180**, 368.
7 E. V. Tsipis, E. N. Naumovich, M. V. Patrakeev, J. C. Waerenborgh, Y. V. Pivak, P. Gaczynski, V. V. Kharton, *J. Phys. Chem. Solids*, 2007, **68**, 1443.
8 V. V. Kharton, A. A. Yaremchenko, A. L. Shaula, M. V. Patrakeev, E. N. Naumovich, D. I. Logvinovich, J. R. Frade, F. M. B. Marques, *J. of Solid State Chem.*, 2004, **177**, 26.
9 H. -S. Kim, H. -I. Yoo, *Phys. Chem. Chem. Phys*., 2012, **12**, 4704.
10 F. A. Kröger, in: *The Chemistry of Imperfect Crystals Vol. 2 2nd revised edition*, North-Holland Publishing Company, Netherlands, 1974.
11 J. D. Jorgensen, B. Dabrowski, S. Pei, D. R. Richards, D. G. Hinks, *Phys. Rev. B*, 1989, **40**, 2187.
12 M. Burriel, G. Garcia, J. Santiso, J. A. Kilner, R. J. Chater, S. J. Skinner, *J. Mat. Chem*., 2008, **18**, 416.
13 J. M. Bassat, P. Odier, A. Villesuzanne, C. Marin, M. Pouchard, *Solid State Ionics*, 2004, **167**, 341.
14 M. Yashima, M. Enoki, T. Wakita, R. Ali, Y. Matsushita, F. Izumi, T. Ishihara, *J. Am. Chem. Soc*., 2008, **130,** 2762.
15 A. Yamada, Y. Suzuki, K. Saka, M. Uehara, D. Mori, R. Kanno, T. Kiguchi, F. Mauvy, J. Grenier, *Adv. Mater*., 2008, **20**, 4124.
16 X.-D. Zhou, J. W. Templeton, Z. Nie, H. Chen, J. W. Stevenson, L. R. Pederson, *Electrochim. Acta*, 2012, **71**, 44.
17 T. Ishihara, N. Sirikanda, K. Nakashima, S. Miyoshi, H. Mtsumoto, *J. Electrochem. Soc.,* 2010, **157**, B141.
18 K. N. Jung, J. H. Jung, W. B. Im, S. Yoon, K. H. Shin, J. W. Lee, *ACS Appl. Mater. Interfaces*, 2013, **5**, 9902.
19 S. Wang, E. Oikawa, T. Hashimoto, *J. Electrochem. Soc*., 2004, **151**, E46.
20 A. Atkinson, T. M.G. M. Ramos, *Solid State Ionics*, 2000, **129**, 259.
21 S. Wang, M. Katsuki, T. Hashimoto, M. Dokiya, *J. Electrochem. Soc*., 2003, **150**, A952.
22 D. Marrocchelli, S. R. Bishop, H. L. Tuller, B. Yildiz, *Adv. Func. Mater*., 2012, **22**, 1958.
23 S. Miyoshi, J. Hong, K. Yashiro, A. Kaimai, Y. Nigara, K. Kawamura, T. Kawada, J. Mizusaki, *Solid State Ionics*, 2003, **161**, 209.
24 M. Kuhn, S. Hashimoto, K. Sato, K. Yashiro, J. Mizusaki, *Solid State Ionics*, 2011, **195**, 7.
25 X. Chen, J. Yu, S. B. Adler, *Chem. Mater.*, 2005, **17**, 4537.
26 S. Hashimoto, Y. Fukuda, M. Kuhn, K. Sato, K. Yashiro, J. Mizusaki, *Solid State Ionics*, 2011, **186**, 37.
27 S. Miyoshi, J. Hong, K. Yashiro, A. Kaimai, Y. Niraga, K. Kawamura, T. Kawada, J. Mizusaki, *Solid State Ionics*, 2002, **154-155**, 257.
28 J. Mizusaki, N. Mori, H. Takai, Y. Yonemura, H. Minamiue, H. Tagawa, M. Dokiya, H. Inaba, K. Naraya, T. Sasamoto, T. Hashimoto, *Solid State Ionics*, 2000, **129**, 163.
29 T. Nakamura, K. Yashiro, K. Sato, J. Mizusaki, *Solid State Ionics*, 2010, **181**, 292.
30 T. Nakamura, K. Yashiro, K. Sato, J. Mizusaki, *Solid State Ionics*, 2010, **181**, 402.
31 Bruker AXS, User's Manual (2008) Bruker AXS, Karlsruhe, Germany.
32 E. J. Opila, H. L. Tuller, *J. Am. Ceram. Soc*., 1994, **77**, 2727.
33 C. Wagner, *Prog. Solid State Chem*., 1971, **6**, 1.
34 T. Nakamura, K. Yashiro, K. Sato, J. Mizusaki, *Solid State Ionics*, 2009, **180**, 1406.
35 R. D. Shannon, C. T. Prewitt, *Acta Crystallogr. B*,1976, **25**, 925.
36 A. Mehta, P. Heaney, *Phys. Rev. B*, 1994, **49**, 563.
37 A. N. Petrov, V. A. Cherepanov, A. Y. Zuyev, V. M. Zhukovsky, *J. Solid State Chem*., 1988, **77**, 1.
38 D. E. Rice, D. J. Buttrey, *J. Solid State Chem*., 1993, **105**, 197.
39 J. M. Tranquada, Y. Kong, J. E. Lorenzo, D. J. Buttrey, D. E. Rice, V. Sachan, *Phys. Rev. B*, 1994, **50**, 6340.
40 M. Hücker, K. Chung, M. Chand, T. Vogt, J. M. Tranquada, D. J. Buttrey, *Phys. Rev. B*, 2004, **70**, 064105.
41 H. Tamura, A. Hayashi, Y. Ueda, *Physica C*, 1996, **258**, 61.
42 S. J. Skinner, *Solid State Science*, 2003, **5**, 419.
43 A. Fossdal, M. Menon, I. Waernhus, K. Wiik, M. Einarsrud, T. Grande, *J. Am. Ceram. Soc*., **87** (2004) 1952.
44 H. Ullmann, N. Trofimenko, T. Tietz, D. Stover, A. Ahmad-Khanlou, *Solid State Ionics*, 2000, **138**, 79.
45 L. W. Tai, M. M. Nasrallah, H. U. Anderson, D. M. Sparlin, S. R. Sehlin, *Solid State Ionics*, 1995, **76**, 273.
46 S. McIntosh, J. F. Vente, W. G. Haije, D. H. A. Blank, H. J. M. Bouwmeester, *Chem. Mater*., 2006, **18**, 2187.
47 Q. Zhu, T. Jin, Y. Wang, *Solid State Ionics*, 2006, **177**, 1199.
48 A. Hisashige, Y. Yamamura, T. Tsuji, *J. Alloys and Comp*., 2006, **408-412**, 1153

Comprehensive studies on the crystal lattice deformation due to interstitial oxygen formation in layered perovskite oxides are presented.